10

Friction Drives with Clutch Capability

Friction drives that also have clutch capabilities are attractive because they are relatively simple and inexpensive. However, they have been inherently limited to relatively low-power applications because of their dependence upon a coefficient of friction that is usually less than 0.6 between the contacting materials. A friction drive was used in an early automobile, but it was discontinued because of its power limitation.

Friction drives recently have been given new life with the development of elastohydrodynamic fluids that become solid under pressure and can change from solid to liquid and back within microseconds. The fluids provide an effective friction coefficient that may be 1.0 or greater as long as the tangential forces impose a shear stress that is less than the ultimate shear stress of the solid-state form of the elastohydrodynamic fluid. Hence, these drives, which feature metal-to-fluid/solid-to-metal contact, can transmit sufficient power to find industrial and automotive applications that benefit from their ability to easily and simply provide continuously variable speeds. At this time they are relatively expensive because of the structure needed to support the large contact forces that induce the fluid-to-solid transformation. They are presently known as *traction drives*. At this time, however, no known traction drives in production include a clutch capability; consequently they will not be included in this chapter.

Several formulas presented in this chapter may be written in nondimensional form for three reasons: (1) the nondimensional form indicates the relative significance of the ratios selected; (2) it allows drive designs to easily be scaled up or down for various applications; and (3) it allows any consistent

set of units to be used for each ratio, and the resulting ratios are independent of the units used.

Relatively broad curves are shown in the following computer-generated graphs for easy reading to show characteristic behavior and to provide contrast against the grid lines. Associated routines, such as Mathcad Trace, appear to read them from the originating data, thereby eliminating the reading errors associated with trace widths.

I. BELT DRIVES

Equipment using nonmetallic belt drives may include the clutch capability by mounting the motor (because it is usually smaller than the driven machine) either upon a hinged base or upon a sliding base fitted with a lever or a linkage that permits the motor to be moved to and from the driven machine in order to apply and relieve the belt tension and thereby give clutching (applying belt tension) and declutching (relieving belt tension) capability.

These designs eliminate the need for a mechanical clutch. Their simplicity is achieved, however, at the risk of introducing the possibility that frictional heating of the belt during idling, when the belt (or belts) may rest on the motor's rotating sheave (pulley). That may generate enough heat to cause belting materials to slowly shrink. This reduction in the center distance between the driving and driven pulleys, or sheaves, may be great enough to cause an unintended re-engagement of the motor and the driven machine. It may also inhibit their disengagement. Consequently, some belt manufacturers produce belts that resist shrinkage due to heating for use in these clutching and declutching applications.

Torque capability for these drives is a separate calculation to be performed according to the procedures given by the belt manufacturers. Therefore, it will not be considered in the following discussion.

A. Hinged Base

At first glance it may appear that moving a motor by mounting it either on a hinged base or on a sliding base is so simple that no analysis is necessary. An analysis, however, does bring forth several considerations that may be missed in selecting the dimensions of the base plate, in locating the position of the base plate hinge, or in designing the linkage for the sliding base plate.

Two similar, but distinct, mounting designs for hinged bases will be considered. In these configurations it is the weight of the motor alone that provides the belt tension. The tension vector shown in Figure 1(a) and (b) acting at the center of the motor shaft represents the sum of the tension acting through the upper and lower belts.

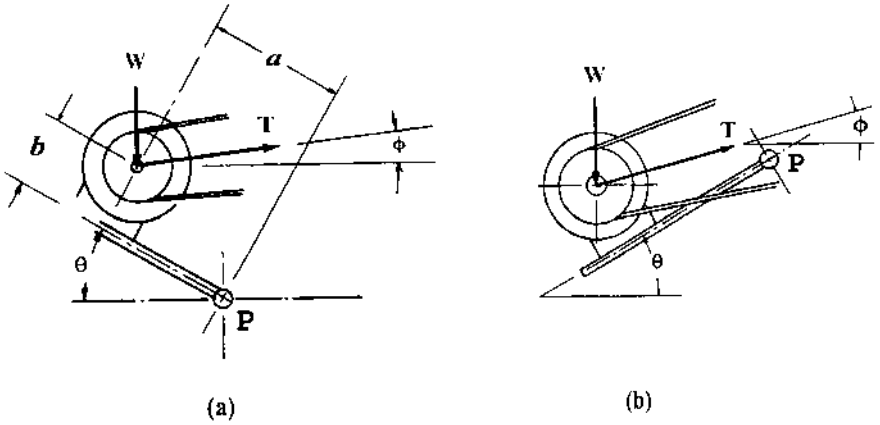

FIGURE 1 Hinged base, belt drive.

Analysis of the first of the two is based upon the configuration shown in Figure 1(a). Upon taking moments about the hinge point P in Figure 1(a) we have

$$W(a\cos\theta - b\sin\theta) = T[a\sin(\theta+\varphi) + b\cos(\theta+\varphi)]$$

After letting $\xi = b/a$, this equation may be written as

$$\frac{T}{W} = \frac{\cos\theta - \xi\sin\theta}{\sin(\theta+\phi) + \xi\cos(\theta+\phi)} \tag{1-1}$$

where θ is positive in the clockwise direction from a horizontal plane through point P and ϕ is positive counterclockwise from a horizontal plane either through or parallel to the motor's axis of symmetry.

Figure 2(a) and (b) show that the weight-to-tension ratio $W/T = 1/(T/W)$ decreases with angle θ when $\phi = 0$. In other words, since W is constant, a decreasing W/T ratio means that tension T increases as θ decreases until θ becomes negative enough for the tension vector **T** to pass through the hinge line that passes through point P. That occurs at the point where $W/T = 0$ on the two lower curves in Figure 2(a). Tension T goes to infinity in Figure 2(b) at those points that are at approximately $\theta = -30.8°$ for $\xi = 0.6$ on the middle curve and at approximately $\theta = -16.6°$ for $\xi = 0.3$ on the lower curve, as determined either by using Mathcad's x – y Trace feature or by interpolation. By comparing the curves in Figure 2(a) it is evident that the W/T ratio also increases as ξ increases for $\phi = 0$ and $\theta = 20°$.

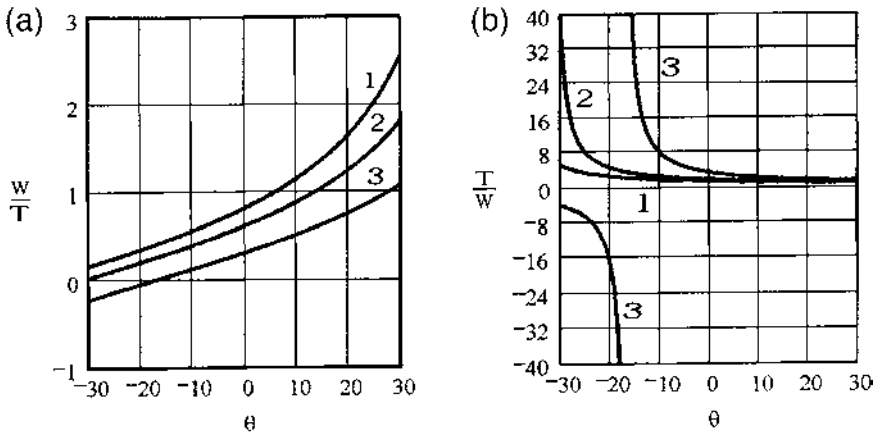

FIGURE 2 Variation of weight-to-tension W/T ratio and tension-to-weight ratio T/W with angle. (a) Plot of W/T, in which $\phi = 0$ for all curves; curve 1, $\xi = 0.8$; curve 2, $\xi = 0.6$; curve 3, $\xi = 0.3$. (b) Plot of T/W, in which $\phi = 0$ for all curves; curve 1, $\xi = 0.3$; curve 2, $\xi = 0.6$; curve 3, $\xi = 0.8$.

Upon turning to Figure 2(b) and recalling that nonmetallic belts under tension stretch over time, it is clear that whenever these belts are used, the tension on them will increase as the angle θ decreases due to the belt's stretching. Hence, the motor must be moved periodically if the tension is to remain within narrow limits.

The rapid increase in tension for negative values of θ in Figure 2(b) emphasizes that the configuration shown in Figure 1(b) should be avoided whenever possible.

A second hinged configuration, shown in Figure 3, differs from the first because the motor base must be supported in the operating, or clutched, position and then lowered for declutching. A cam is shown in Figure 3 as one of several means for lowering the motor for declutching. Some provision must be made, however, to maintain belt tension as the belt stretches.

Upon taking moments about the hinge and letting l represent the distance from the hinge to the support point (from the hinge to the contact between the cam and base plate in Figure 3) we have that

$$Fl = W(a\cos\theta + b\sin\theta) + T[a\sin(\theta+\phi) - b\cos(\theta+\phi)] \qquad (1\text{-}2)$$

Let

$$\eta = \frac{a}{l} \qquad \Lambda = \frac{W}{T} \qquad \zeta = \frac{b}{a}$$

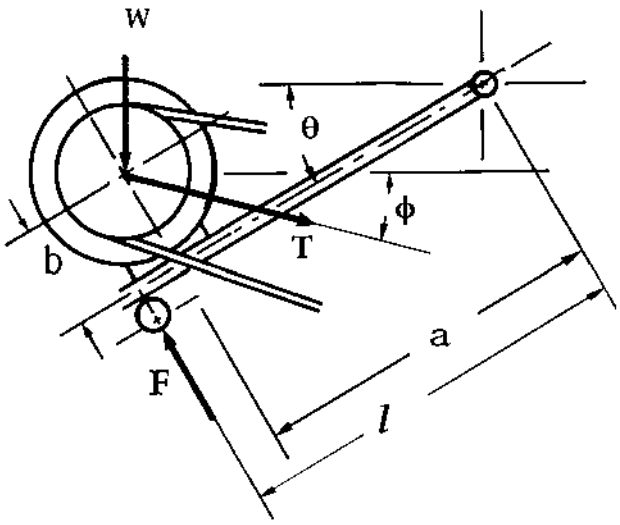

FIGURE 3 Second hinged base configuration, belt drive.

So equation (1-2) may be written in dimensionless form as

$$\frac{F}{T} = \eta[\sin(\theta + \phi) - \zeta \cos(\theta + \phi) + \Lambda(\cos\theta + \zeta \sin\theta)] \tag{1-3}$$

B. Sliding Base

A third mechanism for clutching and declutching involves placing the motor on a sliding base, as shown in the upper drawing in Figure 4, in which the motor base may be both moved back and forth and locked in place by a pair of linkages, one on each side of the sliding base, as shown in the lower drawing in Figure 4. It is locked in place by moving the linkage to a stop below the plane of the slide, as pictured in the lower drawing in Figure 4. This geometry provides a feature not found in the previous two designs: a detent effect on the clutching and declutching force in which the links *a* and *r* will snap into the clutched, or engaged, position after a force maximum is reached. This occurs because the belt is stretched slightly beyond its operating length as the motor base moves back and forth from the declutched to the clutched position of the base.

By summing forces in the horizontal direction acting on the slide upon which the motor is mounted, and assuming that the slide is lubricated so that that the small friction force between sliding surfaces may be ignored in com-

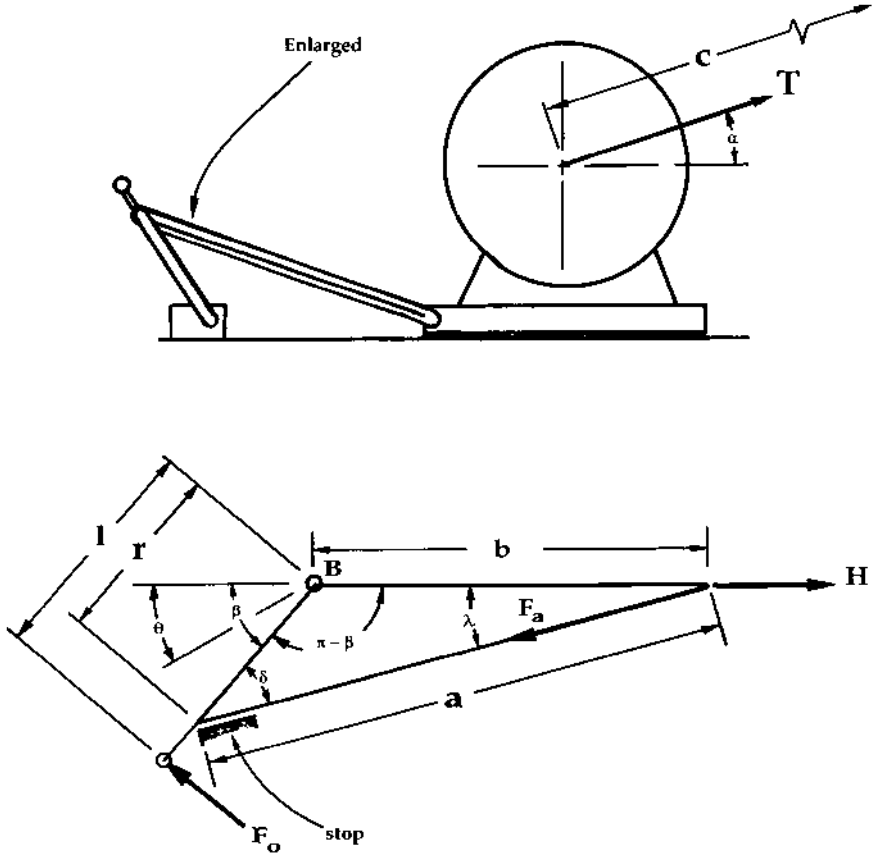

FIGURE 4 Upper drawing: enlarged sketch of sliding motor mount for a belt drive. Lower drawing: linkage geometry.

parison with the belt tension, we find from Figure 4 that the force F_a that acts through link a is related to the horizontal force H acting on the base according to

$$F_a \cos \lambda = H \tag{1-4}$$

where from Figure 4 we also find that

$$H = T \cos \alpha \tag{1-5}$$

The change in angle α as the slide moves is assumed to be small enough relative to changes in angles θ and λ that it may be ignored. Upon taking

moments about pivot B in Figure 4(b) we obtain

$$F_o l = F_a r \sin \delta \tag{1-6}$$

where

$$\begin{aligned} &\delta = \beta - \lambda \qquad \text{in the clutched, or operating, position} \\ &\delta = \theta - \lambda \qquad \text{during de-clutching,} \end{aligned} \tag{1-7}$$

when belt tension is relaxed and where F_o is the force that either the operator or the actuator exerts at the left-hand end of link r. From the law of sines and the geometry in Figure 4, λ is related to θ according to

$$\begin{aligned} &a \sin \lambda = r \sin \theta \qquad \text{in the de-clutched position} \\ &a \sin \lambda = r \sin \beta \qquad \text{in the clutched (operating) position.} \end{aligned} \tag{1-8}$$

After substituting for δ from the second of equation (1-7) into equation (1-6) and then solving for γ from the first of equations (1-8), equation (1-6) may be rewritten as

$$F_o l = F_a r \sin\left[\theta - \sin^{-1}\left(\frac{r}{a} \sin \theta\right)\right] \tag{1-9}$$

Moving the motor away from the driven machine to begin declutching causes the belt to stretch an amount Δc. The corresponding change in length b is given by

$$\Delta b = \Delta c \cos \alpha \tag{1-10}$$

according to the geometry shown in Figure 4.

The force acting on the sliding base during the initial declutching motion as the linkage moves to increase the distance b may be written as

$$H + \Delta H = (T + k\,\Delta c)\cos \alpha = T \cos \alpha + k\,\Delta b \tag{1-11}$$

upon using relation (1-10). In equation (1-11), constant k is the spring for the belt, which is defined by k = force/elongation, hence the force required to strech the belt, which is given by $k\,\Delta c$.

Length Δb may be calculated from the law of cosines, by which the length b may be written in terms of the lengths of links r, a and included angle δ as

$$b^2 = r^2 + a^2 - 2ar \cos \delta$$

Substitution from $\delta = \beta - \lambda$ and from the first of equations (1-7) gives

$$b_o = \left\{r^2 + a^2 - 2ar \cos\left[\beta - \sin^{-1}((r/a)\sin \beta)\right]\right\}^{1/2}$$

at the locked, or clutched, position, and substitution of $\delta = \beta - \lambda$ from the second of equations (1-7) gives

$$b = \left\{r^2 + a^2 - 2ar\cos\left[\theta - \sin^{-1}((r/a)\sin\theta)\right]\right\}^{1/2}$$

Recall that $\theta \leq \beta$ during declutching, and note that both β and θ are positive in the counterclockwise direction from the horizontal plane.

By subtracting b from b_o we have

$$\begin{aligned}\Delta b = &\left\{r^2 + a^2 - 2ar\cos\left[\beta - \sin^{-1}\left(\frac{r}{a}\sin\beta\right)\right]\right\}^{1/2} \\ &- \left\{r^2 + a^2 - 2ar\cos\left[\theta\sin^{-1}\left(\frac{r}{a}\sin\theta\right)\right]\right\}^{1/2}\end{aligned} \tag{1-12}$$

which may be rewritten as

$$\begin{aligned}\Delta b = &a\left\{1 + \Gamma^2 - 2\Gamma\cos\left[\beta - \sin^{-1}(\Gamma\sin\beta)\right]\right\}^{1/2} \\ &- a\left\{1 + \Gamma^2 - 2\Gamma\cos\left[\theta\sin^{-1}(\Gamma\sin\theta)\right]\right\}^{1/2}\end{aligned} \tag{1-15}$$

where $\Gamma = r/a$ and β is the limiting value of θ at the operating position when link a rests against a stop as shown in Figure 4(b). Preparatory to the next substitution, note that the belt's effective spring constant k may be written as $k = T/\varepsilon$, where ε is the elongation of the belt due to tension T.

Substitution from equation (1-12) into equation (1-11) and then into equations (1-4) and (1-9) yields

$$\begin{aligned}\frac{F_o}{T} = \kappa\Big\{&\cos\alpha + \gamma\left[1 + \rho^2 - 2\rho\cos\left(\beta - \sin^{-1}(\rho\sin\beta)\right)\right]^{1/2} \\ &- \gamma\left[1 + \rho^2 - 2\rho\cos\left(\theta - \sin^{-1}(\rho\sin\theta)\right)\right]^{1/2}\Big\} \\ &\times \frac{\sin\left[\theta - \sin^{-1}(\rho\sin\theta)\right]}{\cos\left[\sin^{-1}(\rho\sin\theta)\right]}\end{aligned} \tag{1-13}$$

upon substituting for ka/T according to $ka/T = a/\varepsilon$. Parameters γ and κ are defined by

$$\gamma = \frac{a}{\varepsilon} \qquad \kappa = \frac{r}{l} \qquad \rho = \frac{r}{a} \tag{1-14}$$

By measuring angles in the counterclockwise direction, the force F_o will be positive upward when links a and r are below the horizontal and negative when they are above, indicative of the directions of the initial force to declutch and of the force necessary to keep the linkage in equilibrium when θ goes negative as belt tension is relieved.

Examination of equation (1-13) reveals that κ is a multiplicative constant that decreases the belt tension with increasing lever arm l relative to link r and that γ is a parameter that introduces the effect of belt elasticity.

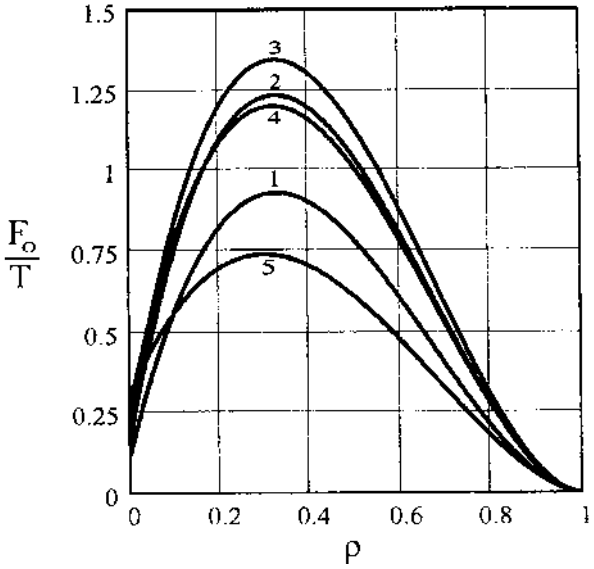

FIGURE 5 Variation of the ratio of operator force to belt tension, F_o/T, with ρ. For all curves, $\kappa = 1$, $\gamma = 1000$, $\alpha = 14°$, and $\beta = 20°$. Angles θ are as follows: curve 1, 6°; curve 2, 9°; curve 3, 12°; curve 4, 15°, and curve 5, 20°.

The plot of F_o/T as a function of ρ in Figure 5 shows that there is an optimum value of ρ that gives the largest detent effect. When $\rho = 0$ there is obviously no belt stretching because $r = 0$ for all finite l. When $\rho = 1$, length r is the same as length a, which implies that they have common pivot points, again making belt stretch impossible. Notice that although the maxima in Figure 5 vary slightly with θ, they lie in the vicinity of $\rho = 0.3$ for the parameters shown.

By plotting F_o/T as a function of θ in Figure 6 we find that the maximum lies at at or close to 12° for $\beta = 20°$. It is also clear that for these values of κ, γ, and β that the choice of β ($\beta \geq \theta$) is important if a detent effect is to be had.

II. FRICTION WHEEL DRIVE

This type of drive, shown in Figure 7, provides both clutch capability and speed variation functions in one pair of discs. This type of friction drive is limited to relatively low-power applications, such as the smaller riding lawnmowers for residential use, because power transfer between discs is limited by the contact force, the friction coefficient, and the shear strength of the tire on

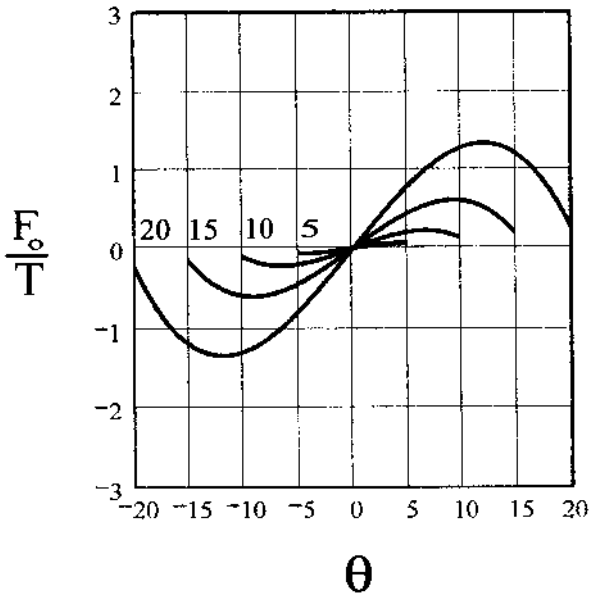

FIGURE 6 Dependence of the ratio of operator force to belt tension, F_o/T, on angle θ. For all curves, $\kappa = 0.001$, $\rho = 0.336$, $\gamma = 1$. Curve 1, $\beta = 20°$; curve 2, $\beta = 15°$; curve 3, $\beta = 10°$; and curve 4, $\beta = 5°$.

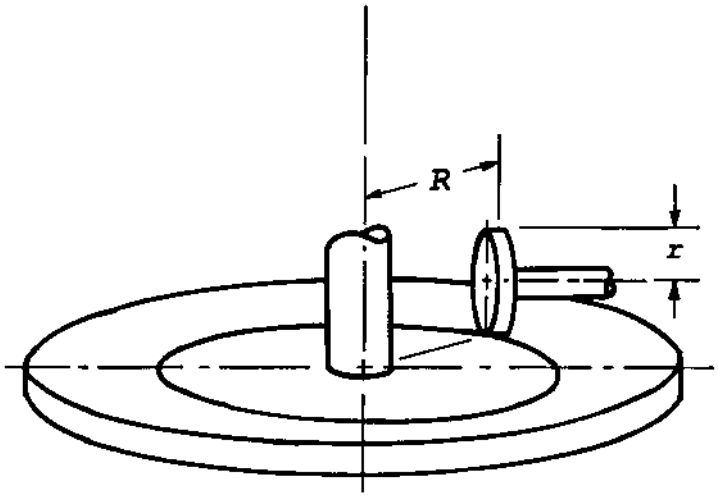

FIGURE 7 Friction drive.

the driven disc. It is an inexpensive alternate to a clutch, bevel gears, and a transmission.

From Figure 7 it follows that the maximum input torque is given by $T_0 = \mu N r$, which is limited by the normal force N and the coefficient of friction μ between the disks. If we let ω_0 and ω_1 represent the angular velocities of the small driver disk and the large driven disk, respectively, it is evident from Figure 7 that the output angular velocity and the maximum output torque T_1 will be given by the following relations if no power is lost due to slippage between the disks; namely,

$$\omega_1 = \omega_0 \frac{r}{R} \quad \text{and} \quad T_1 = T_0 \frac{R}{r} = \mu N R. \tag{2-1}$$

Two possible modes of torque transfer appear possible. In one there may be momentary no-slip contact between the driving and driven discs at some point at or between radii $R - w/2$ and $R + w/2$, where w is the width of the tire on the driven disc. Since the location of this point may change from moment to moment, the driven angular velocity may vary between

$$\omega_{1-} = \omega_0 \frac{R - w/2}{r} \qquad \text{and} \qquad \omega_{1+} = \omega_0 \frac{R - w/2}{r} \tag{2-2}$$

Consequently, the tire may slide over the driver disc except at some point along a line in the contact region. In the other possible mode there may be slip everywhere over the contact region. In the first case, the rotational speed of the driven disc may be found from equation (2-1), and in the second case it will not exceed that given by equation (2-1). Torque transfer may be calculated using the dynamic rather than the static coefficient of friction for the materials involved.

Next, let T_0 denote the torque supplied by the driver disk and T_1 denote the torque transmitted from the driven disk. In terms of the magnitude of the tangential forces $f_{\max}$ or $f_{\min}$ that act between the surface of the driver disk and the tire of the driven disk at their region of contact, we have

$$\begin{aligned} f_{\max}\left(R - \frac{w}{2}\right) &= T_0 \\ f_{\min}\left(R - \frac{w}{2}\right) &= T_0 \end{aligned} \tag{2-3}$$

where $\mu N \geq f_{\max} > f_{\min}$, in which μ is the dynamic coefficient of friction for the materials involved and N is the normal force that presses the driven wheel against the surface of the driving disc. Thus, if the driven wheel is driven at its outer edge,

$$T_{1\min} = r f_{\min} = T_0 \frac{r}{R + w/2} \tag{2-4}$$

and if the driven wheel is driven at its inner edge,

$$T_{1\max} = rf_{\max} = T_0 \frac{r}{R - w/2} \tag{2-5}$$

hence

$$\frac{T_{\max}}{T_{\min}} = \frac{R + w/2}{R - w/2} = \frac{2 + w/R}{2 - w/R} \tag{2-6}$$

If $w/R = 0.1$, then $T_{\max}/T_{\min} = 2.1/1.9 = 1.11$, which is to say that the torque may vary by slightly more than 10%.

Because of the variations in both speed and torque given by equations (2-2) and (2-5), friction drives of this design also may be limited to those systems where the inertia of the driven elements are large enough to effectively average, and thereby smooth, the speed and torque output of the driven unit.

Clutch action is had by raising and lowering the driven disk from and to the driver disk. Speed control is achieved by moving the driven disk in or out to change the value of R in equation (2-1). This type of relatively inexpensive, easily maintained, drive is used to send power to the rear wheels on one manufacturer's line of small riding lawnmowers designed for residential use. Normal force N may be applied by a spring (cantilever, leaf, or coil), and power may be transferred from the small disk by means of a chain or belt arranged to accommodate the changing positions of the small disc relative to the position of the driven component.

III. FRICTION CONE DRIVE

These friction drives are likewise suited for relatively low-power applications and are employed by one manufacturer of zero-turning-radius residential lawnmowers. Contacting components for this drive are shown in Figure 8, where their axes of symmetry are mutually perpendicular and where each cone rotates about its own axis of symmetry. They are sketched in the declutched configuration, in which there is no contact between cones. The driving element is the central double cone having a vertical centerline, and and the driven elements are the individual single cones, one on either side of the driver cone, having horizontal centerlines. Cones having a horizontal centerline are close enough to the driving cone that clutching and declutching is accomplished simply by moving them up or down to contact the driver cone. Directional control of the rotation of the driven cones is selected by moving them to contact either the upper cone or the lower cone of the double-cone driver.

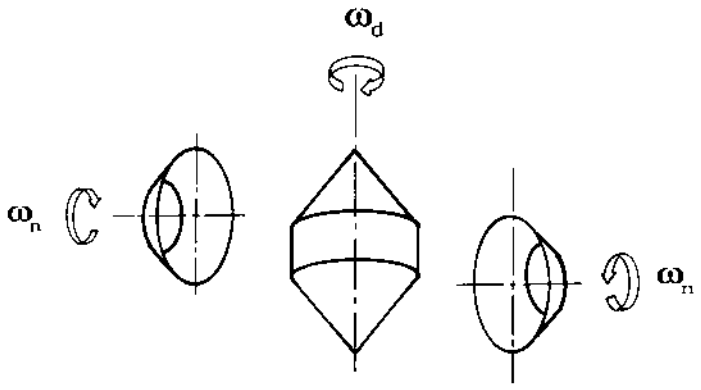

FIGURE 8 Cone friction drive schematic. Central double cone drives output cones on either side.

This type of drive is an inexpensive alternate to bevel gears for a right-angle drive, a clutch, and a reversing mechanism.

When the right-hand cone in Figure 8 is moved downward to contact the upper half of the double cone and the left-band cone is moved upward to contact the lower half of the double cone, both the left- and right-hand cones rotate in the same direction. If the right- and left-hand cones drive the right- and left-hand wheels of a lawnmower, the mower moves forward. If the right-hand cone is moved downward and the left-hand remains downward, the wheels they drive turn in opposite directions and the mower rotates in its own length to provide the zero turning radius. (The unpowered front wheels are on casters.) Finally, if the right-hand cone remains downward and the left-hand cone is moved upward, the mower moves in reverse.

Contact between cones would be along a line where the generators of each cone are in contact if the cones were absolutely rigid. However, the elasticity of the relatively softer cone linings form a contact strip centerd along what would have been the contact line.

Again there are two possible modes of torque transfer; one with no slip at some point or transverse line within the contact region and slip elsewhere, and the other with slip everywhere within the contact area. As illustrated in Figure 9, if slippage at all but one point or line is assumed to occur when two rotating cones are in contact, then the speed of the driven cone will depend upon the location of the no-slip point or transverse line.

From Figure 9 it is evident that with either point or line contact, the angular velocity of the output cones may fall somewhere between the limits determined by the location of that point, or line, within the contact strip where

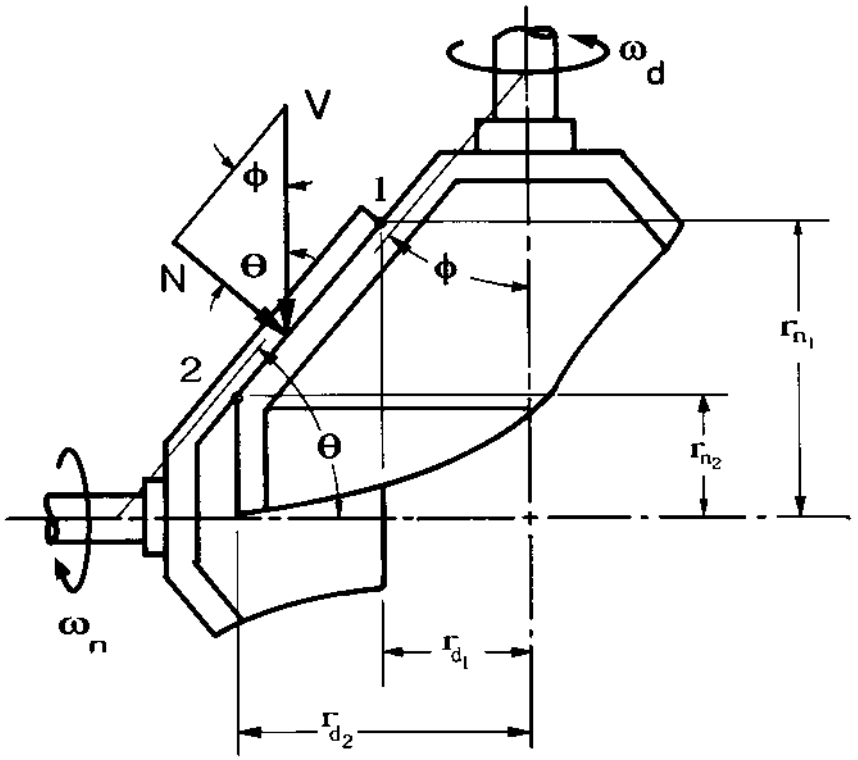

FIGURE 9 Contact between the driver cone and a driven cone.

the two cones may momentarily make contact without slipping. Therefore the angular velocity of an output cone may vary from ω_{n1} to ω_{n2} as given by

$$\omega_{n1} = \frac{\omega_d r_{d1}}{r_{n1}} = \omega_{d1} \frac{l_{d1}}{l_{n1}} \tan^2 \phi \qquad \text{and} \qquad \omega_{n2} = \frac{\omega_d r_{d2}}{r_{n2}} = \omega_d \frac{l_{d2}}{l_{n2}} \tan^2 \phi \tag{3-1}$$

where r_{d1} and r_{n1} are the radii of the driver and driven cones, respectively, at point 1, r_{d2} and r_{n2} are driver and driven radii at point 2, l_{d1}, l_{n1}, l_{d2}, and l_{n2} are the corresponding generator lengths, and $\theta = \pi/2 - \phi$, so that $\tan \theta = \cot \phi$. Angular velocity ω_d is that of the driver cone, and ω_{n1} and ω_{n2} are the angular velocities of a driven cone when driven by contact at points or transverse lines at location 1 or 2, respectively. If there is slip throughout the contact strip, the driven angular velocity will be between the two values for ω_n given in equations (3-1).

It is tacitly assumed that the cones roll smoothly when in contact along a cone generator. This assumption will be valid only if the driving cone fits within the driven cone without interference. Design of cones that will meet this requirement may be begun by returning to the analytical geometry of cones and recalling that the shortest line on the surface of a cone from its apex to it base is called a *generator* of the conical surface and by also recalling that any two-dimensional surface has two principal directions. The radius of curvature is maximum in a plane perpendicular to the surface through one of these principal directions and is minimum in a similar plane through the other principal direction. A generator on a conical surface is the principal direction that has the maximum radius of curvature, infinite, and the minimum radius of curvature of a conical surface at a particular point lies in a plane perpendicular to the generator at that point.

For simplicity in the following discussion, let the minimum radius of curvature of a conical surface be referred to as just the radius of curvature.

From Figure 9 it is evident that for the two cones to fit together without interference, the largest radius of curvature of the driver cone must be equal to, or smaller than, the smallest radius of curvature of the driven cone along their lines of contact. Calculation of the principal radius of curvature in a plane normal to the generator of a cone requires that an expression be obtained for the curve formed by the intersection of the conical surface, as shown in Figure 10(a), and a plane perpendicular to a generator. The equation of a conical surface in the XYZ system shown in Figure 10(b) is

$$X^2 + Y^2 = (Z \tan \phi)^2 \tag{3-2}$$

Substitution for X, Y, and Z in terms of x, y, and z from the coordinate transformation relations corresponding to Figure 10(b) yields

$$\begin{aligned} X &= x \\ Y &= y \cos \theta - z \sin \theta \\ Z &= y \sin \theta + z \cos \theta \end{aligned} \tag{3-3}$$

Equation (3-2) may be written in the x, y, z system by substituting from equations (3-3) into equation (3-2) to get

$$x^2 + (y \cos \theta - z \sin \theta)^2 = (y \sin \theta + z \cos \theta)^2 \tan^2 \phi \tag{3-4}$$

as the equation of a conical surface having a vertex half-angle ϕ whose axis of symmetry lies in the yz-plane and makes an angle θ with the positve z-axis, as shown in Figure 10(a). The equation of the curve formed by the intersection of this conical surface and the plane $z = h$ is found by simply setting $z = h$ in equation (3-4). After this substitution equation (3-4) becomes either the

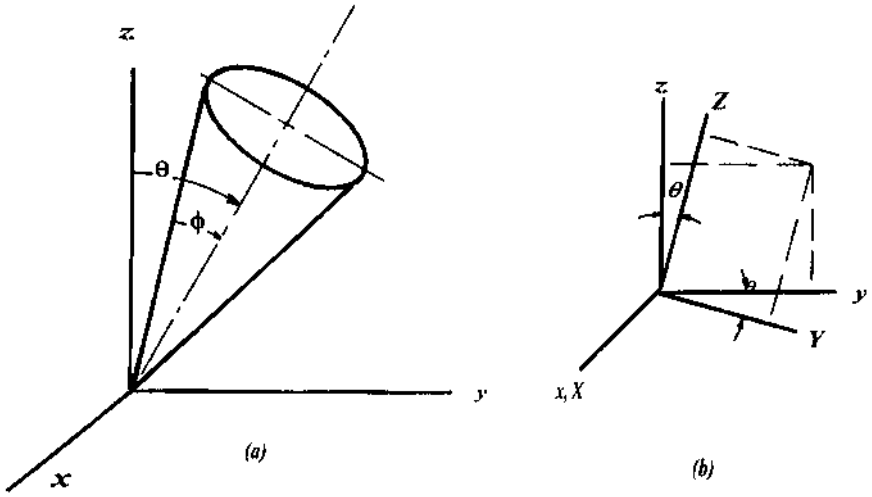

FIGURE 10 Cone geometry and its related coordinates. (a) Cone with vertex at the origin showing radii and angles. (b) Relation between coordinates *X*, *Y*, *Z* and *x*, *y*, *z*.

equation of an ellipse or the equation of a parabola, depending upon the values of θ and ϕ.

Inasmuch as the equation for the radius of curvature ψ of a curve in the xy-plane is given by

$$\psi = \frac{\left[1 + \left(\frac{dy}{dx}\right)^2\right]^{3/2}}{\left(\frac{d^2y}{dx}\right)} \tag{3-5}$$

it is necessary to calculate the first and second derivatives of y with respect to x from equations (3-3). The result is

$$\frac{dy}{dx} = \frac{x}{u} \qquad \text{and} \qquad \frac{d^2y}{dx^2} = \frac{1}{u} - \frac{x}{u^2}\frac{dy}{dx}\left(\tan^2\phi \sin^2\theta - \cos^2\theta\right) \tag{3-6}$$

where

$$u = y\left(\tan^2\phi \sin^2\theta - \cos^2\theta\right) + h\left(1 + \tan^2\theta\right)\sin\theta\cos\theta. \tag{3-7}$$

Let the line of intersection between the driver and driven cones coincide with the z-axis so that $\theta = \phi$ in (3-4), (3-6), and (3-7). Since the driver cone must roll freely within a driven cones, it is essential that its radius of curvature

be less than that of the driven cones all along their lines of contact. This will be the case if the radius of curvature at point 2 in Figure 9 is equal to or less than that of the driven cone at that point.

To satisfy this condition it is necessary to evaluate equation (3-5) at $\theta = \phi = 0$, Figure 10, at the z-value for point 2. A convenient means of doing this and selecting both cones is to plot equation (3-5) as a function of z, as in Figure 11. Examination of Figure 11 shows that satisfactorily mating cones

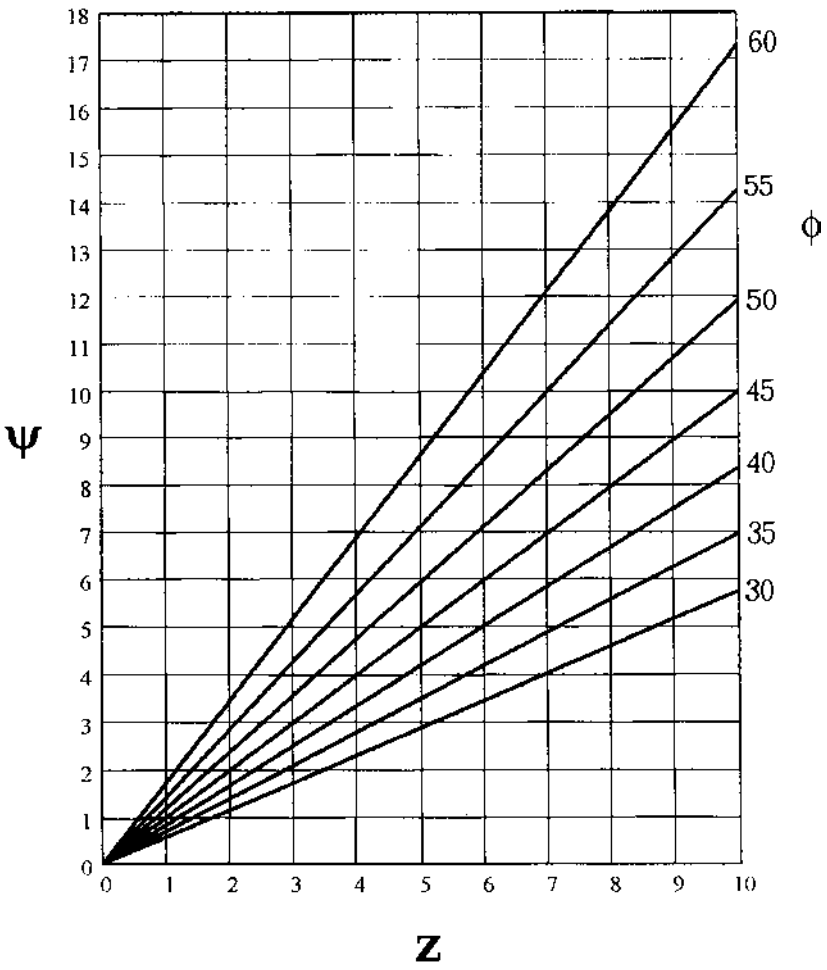

FIGURE 11 Plots of the radius of curvature ρ as a function of distance z from the apex of cones having the included half-angle θ shown. The units of ρ are the units of z.

whose axes of symmetry are mutually perpendicular may be selected in a five-step process. The first step is to choose two half-angles that add to 90°, such as $\phi = 30°$ and $\theta = 60°$. The second step is to select a generator length for the driver cone, z (the one with the smaller included angle), and to read up from that particular z-value to the line corresponding to the half-angle, θ, for that cone. That gives the radius of curvature at that value of z for a cone whose half-angle is θ. The next step is to decide whether the contacting driven cone should have the same radius of curvature at the inner contact point (point 2 in Figure 9) or a larger radius of curvature.

Both choices have consequences. The same radius of curvature may give a slightly broader contact strip about the contact line due to compression of the lining, at least near point *B*. A larger radius of curvature may give greater assurance of no interference.

If the same radius of curvature is selected, step 4 is to move toward the left along the line $\rho = \rho_0$ to the line for the half-angle ϕ of the driven cone. Last, read down to the ordinate to find the corresponding value of z on the driven cone. This completes the fifth step if the same radius of curvature was selected. Otherwise, it is completed by choosing a z-value for a larger ρ-value on the line for the corresponding ϕ.

Selecting $\theta = \phi = 45°$ is a special case. After choosing a particular value of z for the driving cone, select a larger value of z and a correspondingly larger value of ρ for the driven cones in order to allow the driver cone to roll freely inside the driven cones.

In either case, choosing ρ at point 2 in Figure 9 ensures that the driver cone will roll freely inside the driven cone, because ρ of the driver cone decreases as z moves toward the driver cone's apex and ρ for the driven cone increases as z moves outward, away from its apex. This may be verified by plotting x as a function of y from equation (3-4) when written in the form

$$x = \left[(y \sin\theta - z\cos\theta)^2 \tan^2\phi - (y\cos\theta - z\sin\theta)^2\right]^{1/2} \tag{3-8}$$

to get the curves shown in Figure 12 for the z-values selected. As pictured in Figure 12, when the smallest radius of curvature of the driven cone at every point along the contact line (centerline of a contact strip) is larger than the largest radius of curvature for the driver cone at that same point, there is no interference between them at locations away from the contact line because the cone surfaces move away from each other, as indicated by their values as the x-coordinate increases.

Selecting the length of the cylindrical section of the double cone may be accomplished using formula (3-9). It may be written from inspection of Figure 13, which shows the cross sections of half of the driver double cone and half of a driven cone on the left-hand side of the driver cone. From

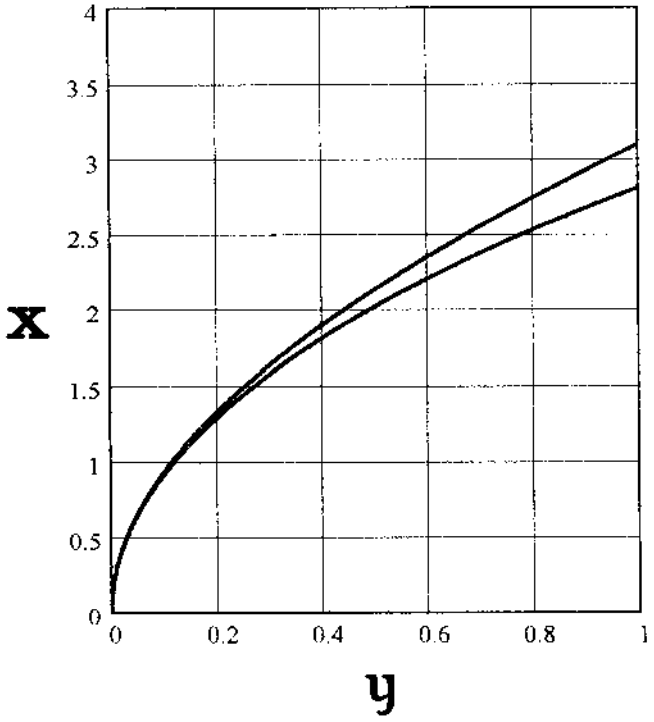

FIGURE 12 Intersection curves of contacting cones with a plane perpendicular to the contact line in terms of the coordinates in Figure 10. Upper curve, $z = 3$ in., $\phi = 55^\circ$ (driver); lower curve, $z = 6$ in., $\phi = 35^\circ$ (driven).

the dimensions shown in that figure, where b is the length of the contact strip, c is the length of the cylindrical section between cones, l_{n1} is the length of a generator on the driven cone, and D is the vertical distance that the driven cone must move vertically to go from contacting the upper driver cone to contacting the lower driver cone, it is evident that D may be written as $D = 2(l_{n1} - b) \sin \theta - c$. Thus,

$$c = 2(l_{n1} - b)\sin \theta - D \tag{3-9}$$

where $(l_{n1} - b)$ is the z-coordinate along the generator of the driven cone to that point where the contact line between the driver and driven cone begins.

Torque that could be transferred to a driven cone for a given dynamic friction coefficient may be estimated from the geometry shown in Figure 9. If the pressure is uniform along the contact line over a small width w, then the

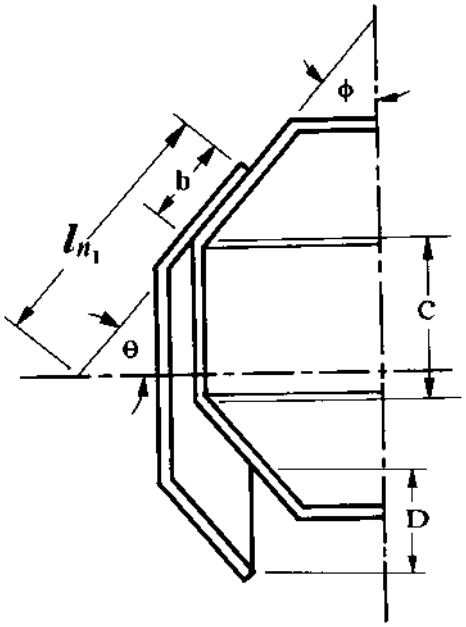

FIGURE 13 Cross sections of a driven cone and half of the driver cone in contact.

maximum torque T that can be contributed by the pressure over an element of length of the contact line may be written as $dT = \mu r\, dN$, where dN is given by $dN = pw\, dl$, r is the radius to the element of length dl, p denotes the pressure, and w represents the width of the lining that is compressed along the contact strip. From Figure 9 it follows that normal force N is related to vertical force V according to $N = V \cos\theta = V \sin\theta$. Thus,

$$dT = \mu r\, dN = \mu pwr\, dl \tag{3-10}$$

where from Figure 9 $dl \sin\theta = dr$, so integration from l_1 to l_2 is equivalent to integration from r_1 to r_2. Hence, from equation (3-10),

$$T = \frac{\mu pw}{\sin\phi}\int_{r_1}^{r_2} r\, dr \tag{3-11}$$

which integrates to

$$T = \frac{\mu pw}{2\sin\phi}\left(r_2^2 - r_1^2\right) = \frac{\mu pw}{\sin\phi}\,\frac{(r_2 + r_1)}{2}\,(r_2 - r_1) \tag{3-12}$$

Substitution from the relations for r_1 and r_2 yields

$$r_2 - r_1 = (l_2 - l_1)\sin\phi \qquad \text{and} \qquad r_2 + r_1 = (l_2 + l_1)\sin\phi$$

So with $pw(l_2 - l_1) = N = V\sin\phi$ we have

$$T = \mu V \frac{l_2 + l_1}{2}\sin^2\phi \tag{3-13}$$

IV. EXAMPLE I: BELT DRIVE, HINGED MOTOR MOUNT

Would you approve a motor mount as illustrated in Figure 1(a) for clutching and declutching? The mass of the motor is 18.6 kg and the center of the motor shaft is 12 cm above the bottom of the motor's base, which is 17.8 cm wide. Center-to-center distance between the shaft of the motor and the shaft of the driven machine is to be 50 cm. Belt tension is to be 298.5 N, the belt should be replaced after the center distance increases 2.4 cm, the angle of the line between centers may be from 15° to 20° with the horizontal, and the shaft of the driven machine is above and to the right of the motor shaft.

The gravitational force on the motor is given by $W = mg$ in terms of the mass of the motor and the acceleration of gravity. Thus

$$W = 18.6(9.8067) = 182.4 \text{ N}$$

to give $T/W = 1.637$. From the motor specifications, $b = 12$ cm and a must be equal to or larger than $17.8/2 = 8.9$ cm. As an aid to selecting a value for a, plot T/W as a function of ξ for $\phi = 20°$ and 30° and for $\theta = 20°$ and 30°, as shown in Figure 14. Select $\phi = 20°$ and compare designs using $\theta = 20°$ and $\theta = 30°$. Use of $\phi = 15°$ was rejected in order to avoid excessive belt tension as the belt stretches. Consider $\xi = 0.2$ to have a larger T/W ratio and consider $\xi = 0.685$, corresponding to $a = 13$ cm, to get a more compact mounting. Thus $a = 44.5$ mm for $\xi = 0.2$ and 13 mm for $\xi = 0.685$.

Since belt elongation during use can alter the geometry shown in Figure 15 by changing angle θ and thereby changing the belt tension, calculate the change in θ due to belt elongation as part of the evaluation of the motor mounting system. Denote the axis of rotation of the motor mount hinge by A, and let c be the center distance between the centerline of the motor shaft and sheave, or pulley, shown on the left-hand side of Figure 15, and the centerline of the input shaft of the driven machine.

From the geometry shown in Figure 15 it is evident that

$$\lambda = \theta + a\tan\xi \tag{3-14}$$

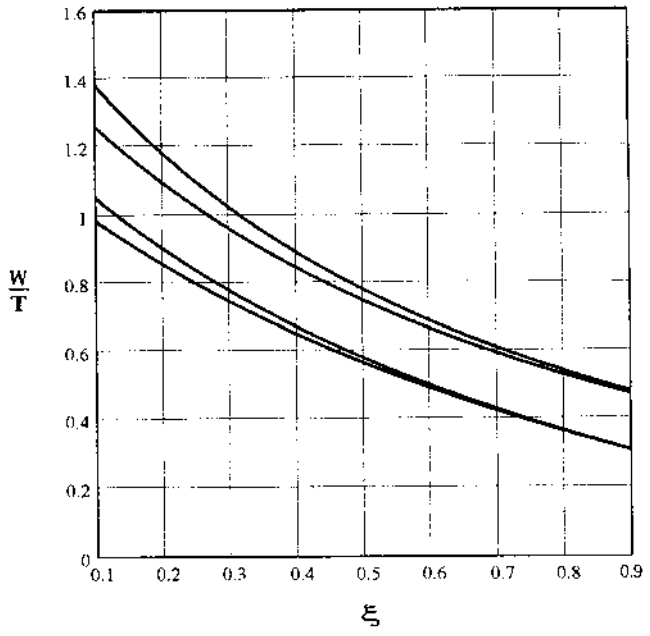

FIGURE 14 Variation of the ratio of the weight to belt tension, *W*/*T*, with the ratio $\xi = b/a$. Upper pair: top curve, $\theta = 20°$, $\phi = 15°$; bottom curve, $\theta = 30°$, $\phi = 15°$. Lower pair: top curve, $\theta = 20°$, $\phi = 20°$; bottom curve, $\theta = 30°$, $\phi = 20°$.

where $\alpha = \tan^{-1}\xi = a\tan\xi$. With this angle known, the law of cosines may be used to find length d from

$$d = \sqrt{h^2 + c^2 - 2hc\,\cos(\lambda + \phi)} \tag{3-15}$$

and from the law of sines,

$$\zeta = a\sin\left(\frac{c}{d}\sin(\lambda + \phi)\right) \tag{3-16}$$

Return to equation (3-15), with center distance c now replaced by c_s, the center distance when the belt is stretched, to calculate the increase in angle ζ which is equal to the decrease in angle θ, since $\theta + \alpha + \zeta$ is a constant. Thus

$$\Delta\theta = \cos^{-1}\left(\frac{h^2 + d^2 - c^2}{2hd}\right) - \zeta \tag{1-17}$$

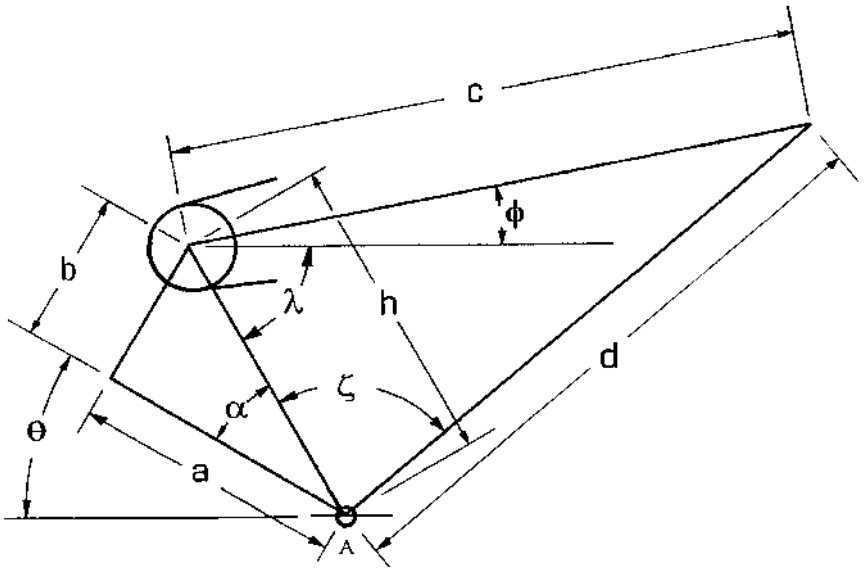

FIGURE 15 Hinged base and motor geometry.

in which ζ represents its value when the belt is new, i.e., as given by equation (3-16).

Call upon equation (1-1) to calculate T/W for the case where $\phi = \theta = 20°$ and $\xi = 0.2$, that is, for $a = 44.5$ cm, to find $T/W = 1.095$. Thus, the tension provided by the weight of the motor is only 199.73 N. Consequently, an additional mass of 9.21 kg must be added to the support to achieve the tension necessary to drive the load. Likewise for $\phi = 20°$ and $\theta = 30°$, the ratio $T/W = 0.434$, which means that weight of the motor alone can induce a tension of only 79.20 N. Thus an additional mass of 51.50 kg must be added. For simplicity of the following calculations, it will be assumed that the weight may be added such that the center of gravity remains along the centerline of the motor shaft.

Substitution into equations (1-14) through (1-17) for $\theta = \phi = 20°$ and $\xi = 0.2$ yields a reduction in θ of 3.930°, which reduces θ to 16.070°, so equation (1-1) gives $T/W = 1.095$. Using the augmented weight added to the motor weight in calculating belt tension when the belt center distance has increased to 52.4 cm gives a belt tension of 329.08 N. For the other design, in which $\xi = 0.685$, $\theta = 30°$, and $\phi = 20°$, equations (1-14) through (1-17) yield an angular reduction of 8.866°, which reduces θ to 21.134°. When the motor and its additional weight are in this position, the belt tension increases to 401.8 N.

If space is available, the choice of $\xi = 0.2$, in which $a = 44.5$ cm, would be preferred because the tension is less sensitive to belt elongation. Belt life may be enhanced in either choice by attaching the hinge to a movable base that can be periodically adjusted to hold θ near 20° as the belt stretches.

V. EXAMPLE 2: BELT DRIVE, SLIDING MOTOR MOUNT

Design a linkage similar to that in Figure 4 for a belt drive for a food grinder in which the operating tension is 173 lb. A line between the centers of the motor and generator shafts lies at an angle of 14° relative to the plane of the slide. The operator's lever arm, link r in Figure 4, should have 3- to 5-inch clearance between the free end of link l and the pin joint connecting it to link a. The belt that will be used stretches 1/32 of an inch when the tension is 173 lb on a freely turning sheave and a detent force of between 3 and 5 pounds.

Plotting F_o as a function of θ reveals that a detent effect is obtained, as is evident from Figure 16, for the parameters listed. Because the desired detent force is much less than 173 lb, initially select $\gamma = 180$; guided by Figure 5, select $\rho = 0.3$. Motivated by Figure 6, choose $\beta = 20°$; and from the

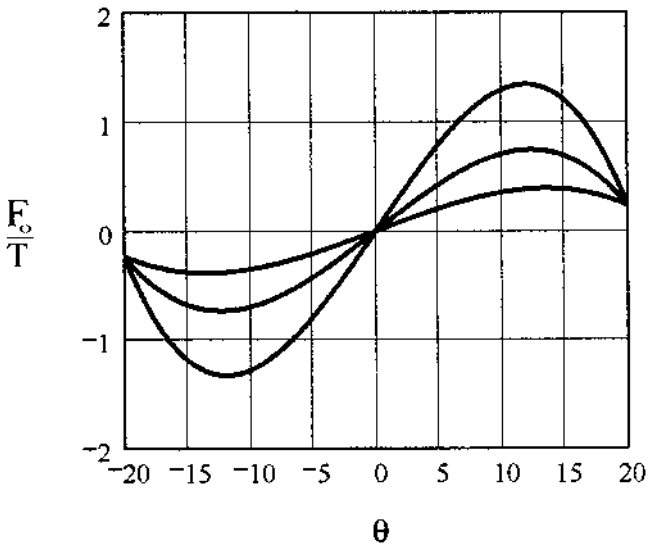

FIGURE 16 Variation of the ratio of operator force to belt tension, F_o/T, with angle θ. $\kappa = 1$, $\gamma = 1000$, $\rho = 0.3$, $\alpha = 14°$, and $\beta = 20°$ for all curves. $\gamma = 1000$ on the largest-amplitude curve, $\gamma = 500$ on the intermediate curve, and $\gamma = 200$ on the smallest-amplitude curve.

maximum in Figure 16, set $\gamma = 13.52°$, as read using the Mathcad Trace feature. Evaluation of equation (1-13) for $\kappa = 0.2$, $\gamma = 180$, $\rho = 0.3$, $\alpha = 14°$, and $\beta = 20$ for $\theta = 13.52°$ and for $\theta = 20°$ gives a detent force of 4.544 lb, which is within the acceptable range. Substitution of $\gamma = 180$ and $\varepsilon = 1/32$ in. into $a = \gamma\varepsilon = 180/32 = 5.625$ in. enables determination of r from $r = \rho a = 0.(5.625) = 1.688$ in. With length l given by $l = r/\kappa = 1.688/0.2 = 8.44$ in., it follows that the clearance given by $l - r = 8.440 - 1.688 = 6.752$ in. exceeds that specified.

This clearance requirement may be satisfied by increasing the magnitude of κ and reducing the magnitude of γ. Thus, if $\kappa = 0.28$ and $\gamma = 150$, the detent force becomes 4.702 lb, a is reduced to 4.688 in., and r becomes 1.406 in. These values give $l = 5.021$ in., so the clearance is $5.021 - 1.406 = 3.615$ in., which is within the desired range.

VI. EXAMPLE 3: CONE DRIVE

Select a cone drive for a combination golf card and a proposed congested area commuter cart for use in communities that accept them. Analysis of torque transmission on the basis of the dynamic coefficients of friction for acceptable linings indicates that a 2.00-in. overlap would be sufficient.

For comparison, consider one design with the driver cone having an apex half-angle of 40° and driven cones having apex half-angles of 50° and a second design in which both the driver and driven cones have apex half-angles of 45°. In both cases initially select a cone generator length of 6.00 in. to allow the overlap to be greater than 2.00 in. in the event that the prototype should require modification.

Begin with the 40°, 50° combination and turn to Figure 11 to select the dimensions of the cones by entering the curve at $z = 6$ and reading up to the 40° line. The principal radius of curvature at that point is 5.0346. Since z is measured in inches, the principal radius of curvature is 5.0346 in. Reading to the left at this value of ρ yields that at $z = 4.25$ in., the principal radius of curvature of the 50° half-angle cone is 5.0650 in. A plot of the x-dimension for each cone, shown in Figure 17(a), confirms that the two cones should roll without interference.

When both the driver and the driven cones have an apex half-angle of 45°, the driver cone may have a generator length of 6.00 in., but the driven cone generator length must be greater in order to have a larger principal radius of curvature. Since the selection of the radii of curvature in the 40°, 50° case differed by 0.0304 in., select the same difference in radii of curvature for the 45°, 45° degree choice, for comparison. From Figure 11 we find that along the 45° line, $z = \rho$; at $z = 6.000$ in., the principal radius of curvature is 6.000 in.; at $z = 6.0304$ in., $\rho = 6.0304$ in. Plotting of the x-dimensions of the two

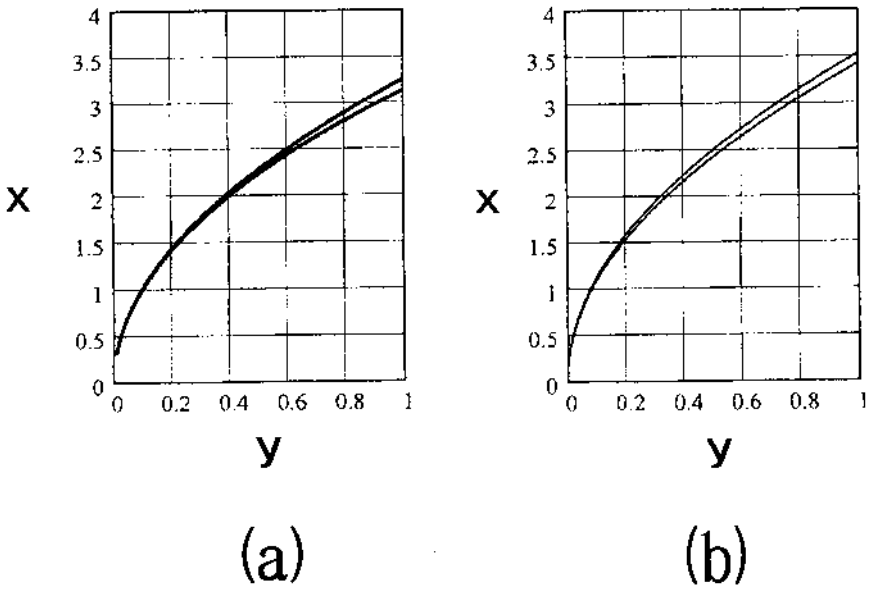

FIGURE 17 Intersection curves of a driver and a driven cone with a plane at the z-values listed. Graph (a): upper curve, $z = 4.25$ in., $\phi = 50°$; lower curve, $z = 6.00$ in., $\phi = 40°$. Graph (b): upper curve, $z = 6.20$ in., $\phi = 45°$; lower curve, $z = 5.8304$ in., $\phi = 45°$.

cones to the scale of Figure 17(a) shows, as might be expected, that the two curves are indistinguishable from one another, because at $y = 1$, their x-values differ by only 0.0088 in. Consequently, compression of the lining between the cones will produce a wider contact strip at this value of z. Calculation of the clearance at a point two in. into the overlap region (i.e., to a point $z = 6.2000$) produces a clearance of 0.107 in. at $y = 1$, which is evident on the scale of Figure 17(a) , as shown in Figure 17(b).

Length of the cylindrical section of the driven cone necessary to have a vertical motion of 0.5 in. for either of these designs may be calculated from equation (3-9). The results are that $c = 4.964$ in. for the 40°, 50° combination and $c = 8.028$ for the 45° pair. Thus, the 40°, 50° pair occupies a smaller volume, reduces the speed of the driven cone, may increase the torque to the driven cone, subject to the restrictions of the lining friction coefficient and the vertical force, and may have a smaller contact region between the cones. Conversely, the 45° pair occupies a larger volume, may give nearly a one-to-one speed ratio, and provides a larger contact area on a compressible lining between the cones.

VII. NOTATION

a,b	length (l)
c	center distance between shafts or cylindrical section, cone drive (l)
D	vertical displacement (l)
F	force (mlt^{-2})
H	horizontal force (mlt^{-2})
k	spring constant (mt^{-2})
l	length (l)
p	pressure ($ml^{-1}t^{-2}$)
R, r	radius (l)
T	torque (ml^2t^{-2}) or tension (mlt^{-2})
W	weight (mlt^{-2})
w	width (l)
α	angle sliding base
β	angle, sliding base
ε	belt elongation (l)
ζ	angle
θ	angle, hinged and sliding bases, driven cone
ϕ	angle, cone half-angle
λ	link angle, sliding base
μ	coefficient of friction
ω	angular velocity (t^{-1})
ψ	radius of curvature (l)

A. Dimensionless Ratios

Λ	W/T
κ	r/l
γ	a/ε
η	a/l
ξ	b/a
ρ	r/a

VIII. FORMULA COLLECTION

Belt drive, hinged base:

$$\frac{T}{W} = \frac{\cos\theta - \xi\sin\theta}{\sin(\theta+\phi) + \xi\cos(\theta+\phi)}$$

Belt drive, supported hinged base:

$$\frac{F}{T} = \eta[\sin(\theta + \phi) - \xi \cos(\theta + \phi) + \lambda(\cos\theta + \xi \sin\theta)]$$

where

$$\eta = \frac{a}{l} \qquad \Lambda = \frac{W}{T} \qquad \xi = \frac{b}{a}$$

Belt drive, sliding base:

$$\frac{F_o}{T} = \kappa\Big\{\cos\alpha + \gamma\big[1 + \rho^2 - 2\,\rho\cos\big(\beta - \sin^{-1}((\rho)\sin\beta)\big)\big]^{1/2} - \gamma\big[1 + \rho^2 - 2\rho\cos\big(\theta - \sin^{-1}((\rho)\sin\theta)\big)\big]^{1/2}\Big\} \times \frac{\sin\big[\theta - \sin^{-1}((\rho)\sin\theta)\big]}{\cos\big[\sin^{-1}((\rho)\sin\theta)\big]}$$

where

$$\gamma = \frac{a}{\varepsilon} \qquad \kappa = \frac{r}{l} \qquad \rho = \frac{r}{a}$$

Speed ratio, friction drive discs:

$$\omega_1 = \omega_0 \frac{R}{r}$$

Torque variation:

$$\frac{T_{\max}}{T_{\min}} = \frac{R + w/2}{R - w/2}$$

Friction drive, cone and plane curve of intersection:

$$x = \left[(y\sin\theta + z\cos\theta)^2 \tan^2\phi - (y\cos\theta - z\sin\theta)^2\right]^{1/2}$$

Cone torque:

$$T = \mu V \frac{l_2 + l_1}{2} \sin^2\phi$$

Cylindrical section length, driver cone:

$$c = 2(l_{n1} - b)\cos\theta - D$$